IEEE JOURNAL OF

# QUANTUM ELECTRONICS

A PUBLICATION OF THE IEEE PHOTONICS SOCIETY

IEEE Photonics Society

APRIL 2018 VOLUME 54 NUMBER 2 IEJQA7 (ISSN 0018-9197)

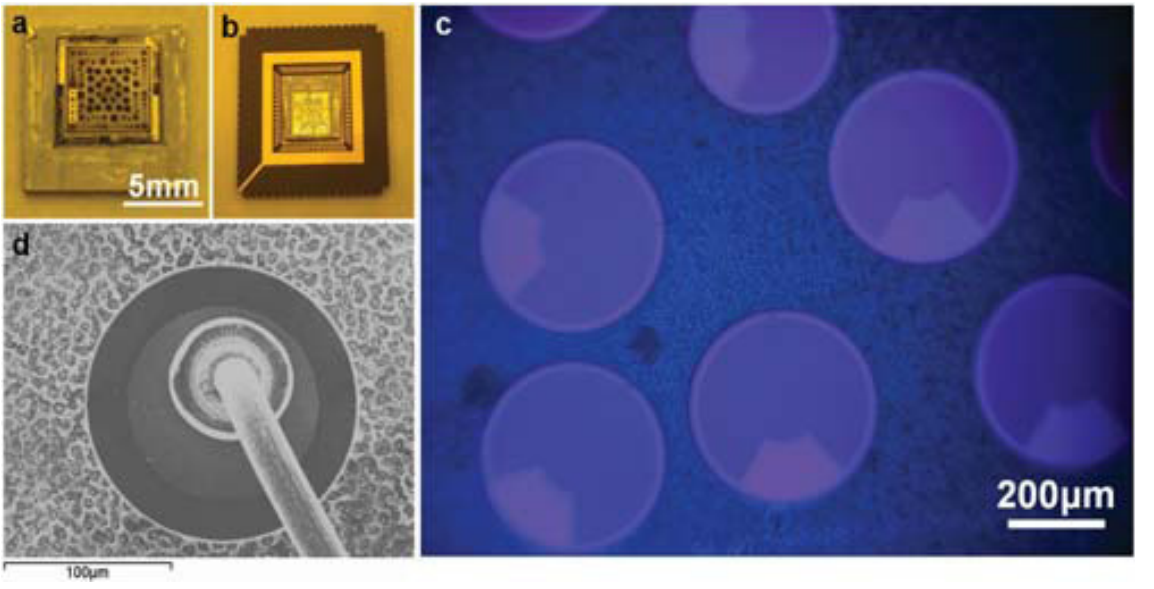


(a) An array of single-element LWIR InAs/$AlAs_{1-x}$ $Sb_x$/$InAs_{1-x}$ $Sb_x$ T2SL photodetectors on Si after the standard processing. (b) Wire-bonded pixels in a 68-pin leadless ceramic chip carrier. (c) An optical photo of transferred LWIR T2SL photodetectors on Si. (d) A SEM image of a wirebonded transferred device (150 $\mu$m) ready for measurement. (Zhang *et al.*, Article #4000207).

IEEE

# Thin-Film Antimonide-Based Photodetectors Integrated on Si

Yiyun Zhang, *Member, IEEE*, Abbas Haddadi, *Member, IEEE*, Romain Chevallier, Arash Dehzangi, *Member, IEEE*, and Manijeh Razeghi, *Life Fellow, IEEE*

***Abstract*— Monolithic integration of antimonide (Sb)-based compound semiconductors on Si is in high demand to enrich silicon photonics by extending the detection range to longer infrared wavelengths. In this paper, we have demonstrated the damage-free transfer of large-area ($1\times1$ cm$^2$) narrow-bandgap Sb-based type-II superlattice (T2SL)-based thin-film materials onto a Si substrate using a combination of wafer-bonding and chemical epilayer release techniques. An array of Sb-based T2SL-based long-wavelength infrared (LWIR) photodetectors with diameters from 100 to 400 $\mu$m has been successfully fabricated using standard "top–down" processing technique. The transferred LWIR photodetectors exhibit a cut-off wavelength of ~8.6 $\mu$m at 77 K. The dark current density of the transferred photodetectors under 200 mV applied bias at 77 K is as low as $5.7\times10^{-4}$ A/cm$^2$ and the R×A reaches 66.3 $\Omega\cdot$cm$^2$, exhibiting no electrical degradation compared with reference samples on GaSb native substrate. The quantum efficiency and peak responsivity at 6.75 $\mu$m (@77 K, 200 mV) are 46.2% and 2.44 A/W, respectively. The specific detectivity (D*) at 6.75 $\mu$m reaches as high as $1.6\times10^{11}$ cm$\cdot$Hz$^{1/2}$/W under 200 mV bias at 77 K. Our method opens a reliable pathway to realize high performance and practical Sb-based optoelectronic devices on a Si platform.**

***Index Terms*— Type-II superlattice infrared photodetectors, epitaxial lift-off, photonics integration.**

## I. Introduction

LONG–WAVELENGTH infrared (LWIR) photodetectors are particularly suitable for terrestrial-based infrared imaging since emission for room temperature objects tends to peak in the 8 to 12 $\mu$m atmospheric window according to Planck's blackbody law. Over the course of the last decade, LWIR imaging has seen tremendous improvement thanks to advances in detector technologies. InAs/GaSb/AlSb Type–II superlattices (T2SLs) have emerged as a highly suitable candidate for LWIR detection due to the ease with which the bandgap can be tuned while retaining closely lattice-matched conditions [1]. They are now directly competing with the state-of-the-art technologies such as mercury cadmium telluride (HgCdTe) compounds [2], [3]. By spatially separating electrons and holes into different quantum wells, the type-II band alignment enables full control of the electronic band structure and allows for great flexibility in the design of hetero-structure devices [4]–[14]. In addition, because T2SLs are a III-V semiconductor material system, the mass production of T2SL-based imagers has the potential to leverage existing commercial III-V foundries to further drive down costs. Another T2SL advantage is its spatial uniformity, already proven in the LWIR band, which is a critical element for the yield of larger high-resolution imagers. Most recently, InAs/AlAs$_{1-x}$Sb$_x$/InAs$_{1-x}$Sb$_x$ T2SLs have been introduced, and they have been shown to have significantly longer minority carrier lifetimes than more conventional InAs/GaSb/AlSb T2SLs; they are actively being pursued as an alternative to InAs/GaSb/AlSb T2SL–based infrared photodetectors and imagers [15]–[22]. Even though they share the same type–II band alignment, these two types of T2SLs exhibit differences in superlattice design. GaSb, AlSb, and InAs all belong to the 6.1Å family, which allows large scale of freedom in the variation of layer thicknesses as well as allowing a variety of novel hetero–structures such as the W-structure [23] or M-structure [24] for pMp [25] or nBn [26] device architectures. On the contrary, AlAs$_{1-x}$Sb$_x$, InAs$_{1-x}$Sb$_x$, and InAs can have very different lattice constants; thus, the constituent layer thicknesses and the antimony molar composition (x) in the AlAs$_{1-x}$Sb$_x$ and InAs$_{1-x}$Sb$_x$ layers need to be taken into account in order to control the strain. This is, especially, true when going to the LWIR and VLWIR regimes where a large antimony molar fraction in the InAs$_{1-x}$Sb$_x$ layers is required [27]. Facing these constraints, the device designers face more challenges in the InAs/AlAs$_{1-x}$Sb$_x$/InAs$_{1-x}$Sb$_x$ T2SLs material system.

Recently, significant efforts have been made to integrate III-V photonic or electronic devices on Si substrates [28]–[32]. There is no doubt that hybrid integration of Sb-based T2SL-based photodetectors on a mature Si photonic platform can extend the applications and utility of the Sb-based material system [33], [34]. Specifically, it will allow for the heterogeneous integrated LWIR detectors on Si. However, it is very difficult to obtain high-performance devices by direct epitaxial growth of Sb-based materials on Si substrates because of the large mismatches in both the lattice constants and thermal expansion coefficients [35], [36]. Therefore, it is desirable to have a simple but reliable method that can lift-off and transfer the Sb-based epi-layers while maintaining the superior performance of the devices.

In the present work, we report the hybrid integration of high-quality large-area LWIR Ga-free

Manuscript received December 5, 2017; revised February 9, 2018; accepted February 14, 2018. Date of publication February 21, 2018; date of current version March 1, 2018. This work was supported by the Defense Advanced Research Projects Agency, Army Research Office under Grant W911NF-16-1-0410. *(Corresponding author: Manijeh Razeghi.)*

The authors are with the Department of Electrical Engineering and Computer Science, Center for Quantum Devices, Northwestern University, Evanston, IL 60208 USA (e-mail: razeghi@eecs.northwestern.edu).

Color versions of one or more of the figures in this paper are available online at http://ieeexplore.ieee.org.

Digital Object Identifier 10.1109/JQE.2018.2808405

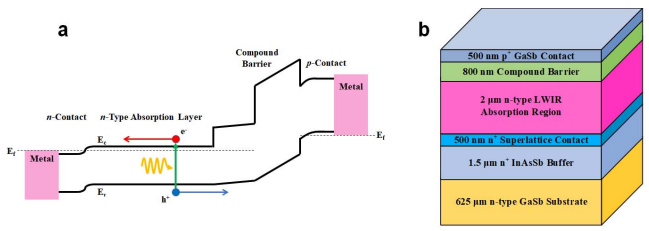


Fig. 1. Schematic diagrams of (a) the device design and (b) the epi-structure for the LWIR InAs/$AlAs_{1-x}Sb_x$/$InAs_{1-x}Sb_x$ T2SL photodetectors.

InAs/$AlAs_{1-x}Sb_x$/$InAs_{1-x}Sb_x$ T2SL thin films and photodetectors onto Si substrates using an epitaxial lift-off method assisted by wafer-bonding techniques. We first introduce the experimental procedures which include the device design and epitaxial growth structure used for the transfer as well as the thin-film transfer process and photodetector fabrication process. Then we will present the detailed characterization of both optical and electrical performance of transferred thin-film photodetectors on Si. Finally, we will discuss the optical response spectrum and the observed oscillations by using simulations and theoretical calculations.

## II. Experimental Procedure

### A. Device Design and Materials Growth

Typical device designs for infrared photodetectors utilize a single electron barrier layer of constant bandgap, whose band structure is specifically chosen to produce a near-zero valence-band offset in order to obtain high-efficiency collection of photo-generated minority carriers. In such a device, the depletion region extends to the narrow-bandgap absorption region which is an important source of generation-recombination dark current. The photodetectors for this study have a $C_pDBn$ architecture (shown in Fig. 1(a)). It consists of an n-doped LWIR T2SL-based absorption region (n) and a large-bandgap p-doped GaSb top contact ($C_p$). Adjacent to the top contact is a thin double electron barrier (DB) which has zero valence band discontinuity with respect to the n-type absorption region. This compound electron barrier is designed to only allow transport of minority carriers (holes) from the absorption region to the top contact; it blocks hole transport in the other direction with a step barrier. To ensure flat-band conditions in the absorber, a compound barrier was used in this experiment such that the electric field in the absorber can be tailored by adjusting the doping in the barrier layer located adjacent to the absorber. This results in a device with reduced dark current and increased sensitivity [37]. The compound barrier consists of a large-bandgap barrier (>1.2 eV) adjacent to the GaSb p-contact and a second smaller electron barrier layer (~300meV) between the first barrier layer and the absorber layer.

The LWIR superlattice absorption region design consists of 26/7 mono-layers (MLs) of InAs/$InAs_{0.52}Sb_{0.48}$, respectively, per period with a ~8 $\mu$m nominal cut-off wavelength at 77K. The small-bandgap electron barrier design consists of 4/3/4/3/4/9 MLs of InAs/AlAs/InAs/AlAs/InAs/$InAs_{0.52}Sb_{0.48}$, respectively, per period with a nominal cut-off wavelength of ~4 $\mu$ m. We call this structure a saw-tooth superlattice. An $AlAs_{0.52}Sb_{0.48}$/GaSb superlattice is used as the large-bandgap electron barrier. The addition of this second barrier pushes part of the depletion region into the larger bandgap region, decreasing the generation-recombination (G-R) current. The larger bandgap barrier also helps suppress surface band-bending and associated surface leakage [37]. Ternary $AlAs_{0.52}Sb_{0.48}$ was used in the superlattice design because it is lattice–matched to the GaSb substrate and has antimony (Sb) atoms in common with GaSb; this provides a great deal of flexibility in the superlattice design and eliminates the need for any special interface design or strain balancing. Because of the common–anion rule of band lineups, the valence–band offset between $AlAs_{0.52}Sb_{0.48}$ and GaSb is small, which is the desired situation to allow smooth hole transport. The electron quantum well in an $AlAs_{0.52}Sb_{0.48}$/GaSb superlattice is deep (~1.19 eV), however, which allows for large bandgaps in the range of ~0.8 to ~1.6 eV. Furthermore, using an $AlAs_{0.52}Sb_{0.48}$/GaSb superlattice as the electron barrier layer results in a smoother surface morphology compared to the case in which the barrier layer consists of a simple ternary AlAsSb layer. Finally, the growth conditions for $AlAs_{0.52}Sb_{0.48}$/GaSb superlattices are exactly the same as for the InAs/ $InAs_{0.52}Sb_{0.48}$ absorption region, which allows for straightforward integration of these components. We call this structure an H-structure superlattice. The electron barrier H-structure superlattice design consists of 5/2 MLs of $AlAs_{0.10}Sb_{0.90}$/GaSb, respectively, with a bandgap energy of ~1.2 eV at 77 K.

The device was grown on a Te-doped n-type ($10^{17}cm^{-3}$) GaSb wafer using a solid source molecular beam epitaxy (SSMBE) reactor equipped with group III SUMO® cells and group–V valved cracker cells. The growth started with a 100 nm GaSb buffer layer to smooth out the surface, then, a 1.5 $\mu$m n-doped $InAs_{0.91}Sb_{0.09}$ buffer layer ($10^{18}cm^{-3}$) was grown, which was followed by the 0.5 $\mu$m n-contact ($10^{18}cm^{-3}$), the 2 $\mu$m-thick n-type absorption region ($10^{15}cm^{-3}$), the 0.8 $\mu$m compound electron barrier, and the 0.5 $\mu$m p-contact (see Fig. 1(b)). Silicon (Si) and Beryllium (Be) were used as the n- and p-type dopants, respectively.

### B. Thin-Film Transfer Procedure

Fig. 2 shows schematic diagrams of the process flow for transferring the LWIR InAs/$AlAs_{1-x}Sb_x$/$InAs_{1-x}Sb_x$ T2SL photodetectors onto a Si substrate. First, the samples were degreased with ultrasonic cleaning in organic solvents. A layer of Ti/Au (40nm/120nm) was then deposited on the both the Si and InAs/$AlAs_{1-x}Sb_x$/$InAs_{1-x}Sb_x$ T2SL wafers by electron-beam evaporation. The Ti/Au layer on the T2SL serves both as a bottom contact and as a metallic reflector for the incident light. Both Ti/Au layers were then covered with a 1.5 $\mu$m-thick indium film which was then thermally evaporated on this Ti/Au layer to be used as a bonding layer. After that, the InAs/$AlAs_{1-x}Sb_x$/$InAs_{1-x}Sb_x$ T2SL and Si wafers were diced into 1×1 $cm^2$ and 2 × 2 $cm^2$ pieces,

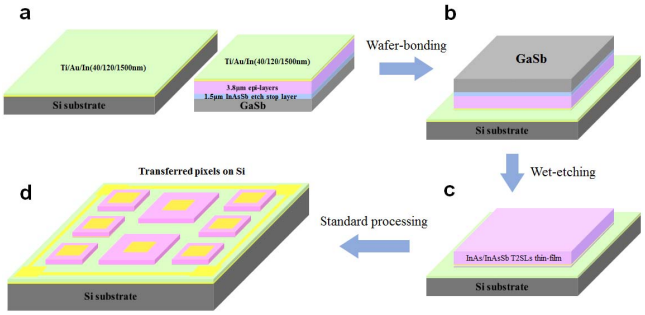


Fig. 2. Schematic diagram of the process flow for transferring the LWIR $InAs/AlAs_{1-x}Sb_x/InAs_{1-x}Sb_x$ T2SL photodetectors to a Si substrate (a–c) and then fabricating detectors via standard processing (d).

respectively. A wafer-bonding process was then carried out for 20 min at room temperature with a force of 160 kg applied; this allows the wafers to be bonded firmly. After wafer bonding, wax was applied around the periphery of the $InAs/AlAs_{1-x}Sb_x/InAs_{1-x}Sb_x$ T2SL wafer to protect the indium and edges of the wafer while leaving the back of the GaSb substrate exposed. The protected hybrid-wafer was then emerged into a $CrO_3$/HF etching solution to remove the GaSb substrate. This etchant offers excellent etch selectivity between GaSb substrate and $InAs_{1-x}Sb_x$ buffer layer, which effectively terminates the wet-etching process at the substrate/buffer layer interface. After the GaSb substrate was totally removed, the wafer was taken out and rinsed in deionized (DI) water and the wax was removed with hot trichloroethylene (TCE) (80 °C). The wafer was then cleaned in an ultrasonic bath with acetone and then blown dry with nitrogen. After this GaSb substrate removal process, the transferred thin-film was assessed using high resolution X-ray diffraction (HR-XRD) and atomic force microscopy (AFM).

### *C. Device Fabrication and Testing*

The transferred T2SL material was then processed into single-element $InAs/AlAs_{1-x}Sb_x/InAs_{1-x}Sb_x$ T2SL unpassivated circular and square-shaped photodetectors with sizes ranging from $100 \times 100$ $\mu m^2$ to $400 \times 400$ $\mu m^2$ using standard processing techniques, including a two-step (dry followed by wet etching) mesa definition process and deposition of metallic top/bottom electrodes (Ti/Au) [19], [20] The two-step mesa definition process consists of dry-etching via inductively-coupled plasma (ICP) in an Oxford Plasma Lab System 100, followed by a 90 second citric acid-based wet-etch to remove the ion-induced damage and surface traps on the pixel sidewalls. Silicon pieces containing processed detector pixels were placed in 68-pin leadless ceramic chip carriers (LCCC), and individual photodetectors were wire bonded for testing. Chip carriers were then loaded into a cryostat for both optical and electrical characterizations at 77 K. The optical characterization of these LWIR photodetectors was performed under front-side illumination with no anti-reflection coating. A Bruker IFS 66v/S Fourier transform infrared spectrometer (FTIR) was used to measure the spectral response and a calibrated blackbody source at 1000 °C was used to calibrate the responsivity and quantum efficiency.

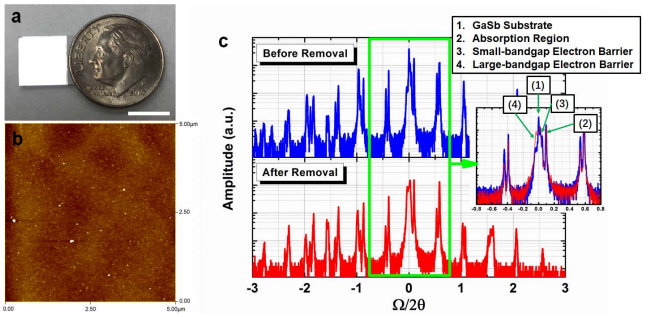


Fig. 3. (a) A $1 \times 1$ $cm^2$ $InAs/AlAs_{1-x}Sb_x/InAs_{1-x}Sb_x$ T2SL-based thin-film transferred onto a Si substrate (The scale bar is 1 cm and a US dime is also shown for size comparison). (b) Atomic force microscopy of a $5 \times 5$ $\mu m^2$ surface area of the transferred material with an RMS roughness value of 4.47 Å. (c) High-resolution X-ray diffraction of the materials before/after the transfer (inset: detail view showing just the zero-order peaks of the T2SLs, compound barriers and GaSb substrate/contact layer).

## III. Results and Discussions

A large-area ($1 \times 1 cm^2$) $InAs/AlAs_{1-x}Sb_x/InAs_{1-x}Sb_x$ T2SL-based thin-film transferred to a Si substrate is shown Fig. 3(a), with a US dime shown for size comparison. The Si surrounding the transferred Sb-based thin-film has been removed via dicing. The mirror-like surface of the transferred thin-film is continuous and crack-free, which shows the excellent quality of the wafer-bonding and chemical substrate removal. Atomic force microscopy shows a good surface morphology with a root mean squared (RMS) roughness of 4.47 Å over a $5 \times 5$ $\mu m^2$ area (see Fig. 3(b)). High-resolution X-ray diffraction (HR–XRD) scans show that the films are almost identical before and after transfer (see Fig. 3(c)). The position of all the peaks for the transferred thin-film are completely consistent with the peaks from the as-grown thin-film, suggesting that no relaxation has occurred after the transfer process. The inset of Fig. 3(c) overlays both scans in a narrow range and shows the expected decrease in the zero-order GaSb peak intensity due to the GaSb substrate having been completely removed during the substrate removal process. The remaining GaSb peak after transfer is due to the GaSb p-contact layer. The lattice mismatch to the GaSb substrate of absorption region, small-bandgap electron barrier, and larger bandgap barrier is −1500, −480, and 490 ppm, respectively, as is expected.

Fig. 4(a) shows an optical image of an array of $InAs/AlAs_{1-x}Sb_x/InAs_{1-x}Sb_x$ T2SL-based pixels on Si after processing. Even with 1 hour of ultrasonic cleaning, there is no loss in the number of hybridized pixels with sizes ranging from $100 \times 100$ $\mu m^2$ to $400 \times 400$ $\mu m^2$, demonstrating that the transferred pixels are bonded very well to the Si substrate. This is significant for the integration of IR imaging devices onto a Si platform, which will require an enormous number of micro-pixels for high resolution. Moreover, the sidewalls of the transferred pixels are totally fresh and clean after the mesa definition and cleaning process, suggesting that good electrical properties can be obtained. Fig. 4(c) shows a closeup view of the mesa-isolated LWIR $InAs/AlAs_{1-x}Sb_x/InAs_{1-x}Sb_x$ T2SL photodetectors on Si substrate. A SEM image of a 150$\mu$m wire-bonded pixel on the chip carrier is presented in Fig. 4(d).

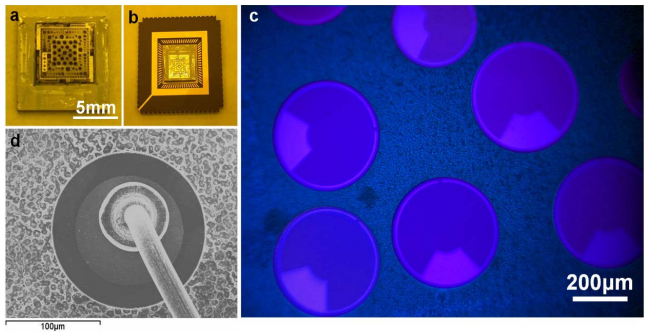


Fig. 4. (a) An array of single-element LWIR InAs/AlAs$_{1-x}$Sb$_x$/InAs$_{1-x}$Sb$_x$ T2SL photodetectors on Si after the standard processing. (b) Wire-bonded pixels in a 68-pin leadless ceramic chip carrier. (c) An optical photo of transferred LWIR T2SL photodetectors on Si. (d) A SEM image of a wire-bonded transferred device (150 $\mu$m) ready for measurement.

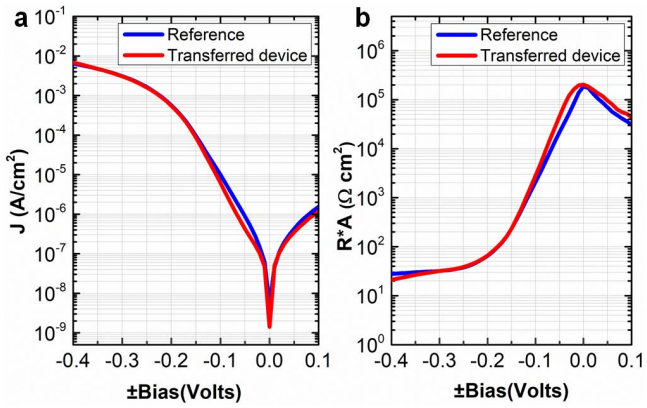


Fig. 5. (a) Dark current density and (b) differential resistance×area (R×A) product vs. applied bias voltage of a typical transferred photodetector on Si and a reference sample on native GaSb substrate at 77 K.

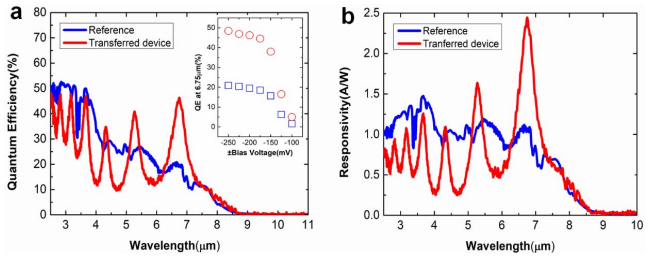


Fig. 6. (a) Saturated quantum efficiency spectra of the transferred device and reference sample at 200mV applied bias voltage in front-side illumination configuration without any anti-reflection coating. Inset shows quantum efficiency of the devices at 6.75 $\mu$m in front-side illumination configuration as a function of applied bias voltage.

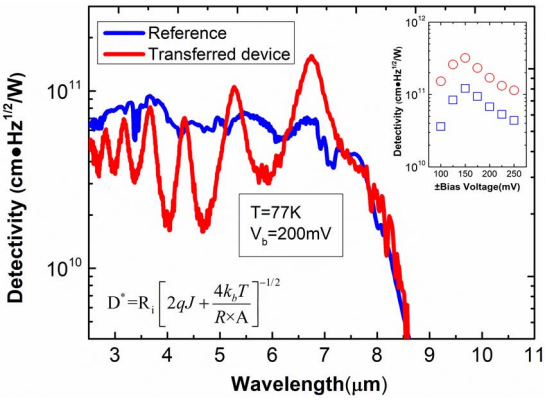


Fig. 7. Specific detectivity (D*) spectrum of the transferred devices on Si and of a reference sample on native GaSb substrate at 200 mV applied bias voltage, at 77K. Top-right inset shows the detectivity versus bias at 6.75$\mu$m. The specific detectivity is calculated based on the equation in the bottom-left inset, where $R_i$ is the device responsivity, $J$ is the dark current density, R×A is the differential resistance×area product, $k_b$ is the Boltzmann constant, and $T$ is the operating temperature.

Fig. 5(a)-5(b) shows the current-voltage characteristic and differential resistance×area (R×A) product of the transferred LWIR T2SL photodetectors on Si and reference sample on native GaSb substrate at 77K. Unlike other transfer methods resulting in conspicuous degradation in the electrical performances, [38], [39] by using the proposed epitaxial liftoff (ELO) method in this work, the dark-current characteristics of the transferred LWIR T2SL photodetectors on Si are almost identical to that of reference samples on native substrate, demonstrating that the electrical properties do not degrade after the InAs/AlAs$_{1-x}$Sb$_x$/InAs$_{1-x}$Sb$_x$ T2SL photodetectors are transferred. Specifically, the dark current density of the transferred LWIR T2SL photodetectors at a forward bias of 200mV is as low as $5.7 \times 10^{-4}$ A/cm$^2$ and the corresponding R × A product reaches 66.3 Ω·cm$^2$. The low dark current density is attributed to the good cleaning of the sidewalls during the processing. Because of the flipped structure, the reference devices are driven in the opposite polarity to the transferred devices, but the bias has been reversed in the graphs to make a better comparison.

Fig. 6 shows the quantum efficiency for the transferred photodetectors and reference sample on the native GaSb substrate. The cut-off wavelength is around 8.6 $\mu$m, which is consistent with the material design. The peak quantum efficiency and responsivity (@200mV) emerging at a wavelength of 6.75$\mu$m are about 46.2% and 2.44 A/W, respectively, which are 2.3 times higher than that of the reference sample. As the bias increases from 200 to 250mV, a maximum quantum efficiency of ~49% is obtained.

After performing both optical and electrical characterization, the specific detectivity (D*) was calculated for the transferred LWIR photodetectors at 77K. Fig. 7 shows the calculated detectivity for the transferred LWIR T2SL photodetectors on Si and for a reference sample on native GaSb substrate. The peak detectivity at 6.75$\mu$m is $1.6\times10^{11}$ cm·Hz$^{1/2}$/W at a forward bias of 200 mV, which is 2.4 times higher than that of the reference sample. The maximum detectivity reaches as high as $3.2\times10^{11}$ cm·Hz$^{1/2}$/W at a forward bias of 150mV, as shown in the top-right inset of Fig. 7.

For these substrate-transferred thin-film Sb-based photodetectors, there is a clear oscillation throughout the optical response spectrum due to Fabry-Perot resonances within the thin-film device. Fig. 8(a) shows the photoresponse and simulated transmission spectra from a 3.81$\mu$m-thick pixel transferred on Si. The height of 3.81 $\mu$m is obtained from the measurement with an optical profiler, as shown in inset of Fig. 8(a). The oscillations observed in the photoresponse spectra are consistent with the Fabry-Perot modes confined

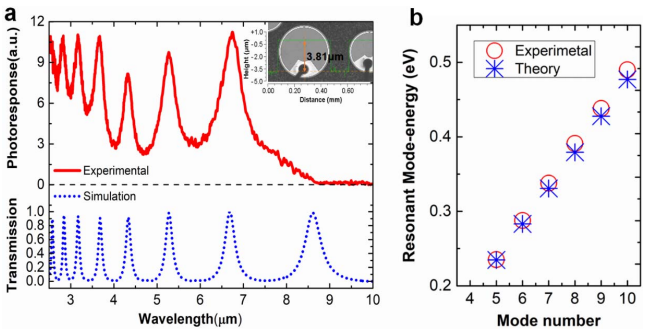


Fig. 8. (a) Photoresponse and simulated transmission spectra from a 3.81$\mu$m-thick pixel transferred on Si. (b) Experimental photoresponse and calculated transmission oscillations for incoming light. Inset shows the height of the transferred pixels from optical profilometry.

within InAs/AlAs$_{1-x}$Sb$_x$/InAs$_{1-x}$Sb$_x$ T2SL thin-film photodetectors on Si from the two-dimensional finite-difference time-domain (2D-FDTD) simulation. Here, the 2D-FDTD optical simulations were carried out for the Sb-based T2SL thin-film structure, which has a measured thickness of 3.81 $\mu$m and a width of 100 $\mu$m. A plane-wave with a wavelength range of 2-10 $\mu$m was used as the incident light source, which is placed 15 $\mu$m from the Sb-based materials. A frequency domain field and power monitor was placed inside the InAs/AlAs$_{1-x}$Sb$_x$/InAs$_{1-x}$Sb$_x$ T2SL thin-film to check the transmission spectra. An Ti/Au (40nm/150nm) layer sequence was placed at the bottom of the Sb-based T2SL thin-film. The simulation domain was set with a width of 100 $\mu$m and with 50 $\mu$m in thickness, with periodic boundary conditions and perfectly matched layers. The effective refraction index of the Sb-based T2SL was chosen from fitting experimental data. No optical absorption was considered in the simulations. The confinement originates from the reflections that occur between the Ti bottom contact and the InAsSb/air interface. In general, the resonant wavelengths for different mode numbers (m=4, …, 10) can be calculated with the relationship:

$$m\lambda/2 = n(\lambda) \times L,$$

where n($\lambda$) is the dispersive refractive index and $L$ is the thickness of the T2SL photodetectors transferred onto Si. Fig. 8(b) shows that the calculated transmission peaks match well with the experimental results, which further confirms that the oscillations in the photoresponse spectra are attributed to Fabry-Perot resonances. It is worth noting that these Fabry-Perot oscillations will be reduced and a nearly flat response spectrum from these substrate-transferred on-chip thin-film photodetectors can be expected if a broadband anti-reflection coating is applied to the InAsSb/air interface. In addition, one probable reason that it cannot be observed such enhancement at shorter wavelengths is due to the Ti/Au reflector at the bottom has a lower reflectivity for the short-wavelength infrared range. Therefore, the performance of these substrate-transferred detectors will be further improved with better optical designs to reduce the loss at the metallic contact interface with the Sb-based materials and application of an anti-reflection coating to the top surface.

## IV. Conclusion

In summary, an array of high-performance LWIR Ga-free InAs/AlAs$_{1-x}$Sb$_x$/InAs$_{1-x}$Sb$_x$ T2SL photodetectors were successfully integrated onto Si substrate through wafer bonding of 1×1 cm$^2$ thin films, substrate removal, and standard device processing. These transferred devices displayed a cut-off wavelength of 8.6 $\mu$m at 77 K. At the peak response of 6.75 $\mu$m, the transferred photodetector revealed a quantum efficiency and responsivity of 46.2% and 2.44 A/W at 200mV bias, respectively, when it was under front-side illumination and with no anti-reflection coating. The dark current density of the transferred photodetectors under 200 mV bias at 77K reached $5.7\times10^{-4}$ A/cm$^2$, exhibiting no electrical degradation compared to reference samples on native GaSb substrates. The devices also demonstrated a saturated dark current shot noise limited specific detectivity of $1.6\times10^{11}$ cm·Hz$^{1/2}$/W at 6.75 $\mu$m, under 200mV bias, at 77 K. Being compatible with traditional semiconductor processing techniques, this reliable large-area transfer method and high-yield fabrication of high-performance Sb-based T2SL micro-pixel photodetectors on Si substrates will allow new applications for this material system. This technology offers a straightforward, yet simple, technique for hybrid integration of Sb-based T2SL photodetectors with silicon readout integrated circuits (ROIC) for focal plane array (FPA) imaging applications. In addition, this work also presents a feasible solution for heterogeneous integration of high-performance Sb-based electronic devices like high electron mobility transistors (HEMTs) and metal-oxide-semiconductor field-effect transistors (MOSFETs) on a Si microelectronics platform.

## Acknowledgment

The views and conclusions contained in this document are those of the authors and should not be interpreted as representing the official policies, either expressed or implied, of the Defense Advanced Research Projects Agency, Army Research Office or the U.S. Government. The U.S. Government is authorized to reproduce and distribute reprints for Government purposes notwithstanding any copyright notation herein.

## References

[1] G. A. Sai-Halasz, R. Tsu, and L. Esaki, "A new semiconductor superlattice," *Appl. Phys. Lett.*, vol. 30, no. 12, pp. 651–653, 1977.

[2] M. Razeghi, A. Haddadi, A. Dehzangi, R. Chevallier, and T. Yang, "Recent advances in InAs/InAs$_{1-x}$Sb$_x$/AlAs$_{1-x}$Sb$_x$ gap-engineered type-II superlattice-based photodetectors," *Proc. SPIE*, vol. 10177, p. 1017705, May 2017.

[3] M. Razeghi *et al.*, "Advances in antimonide-based type-II superlattices for infrared detection and imaging at center for quantum devices," *Infr. Phys. Technol.*, vol. 59, pp. 41–52, Jul. 2013.

[4] M. Razeghi *et al.*, "Antimonide-based type II superlattices: A superior candidate for the third generation of infrared imaging systems," *J. Electron. Mater.*, vol. 43, no. 8, pp. 2802–2807, 2014.

[5] M. Razeghi, S. A. Pour, E. Huang, G. Chen, A. Haddadi, and B. Nguyen, "Type-II InAs/GaSb photodiodes and focal plane arrays aimed at high operating temperatures," *Opt-Electron. Rev.*, vol. 19, no. 3, pp. 261–269, 2011.

[6] A. M. Hoang, G. Chen, A. Haddadi, S. A. Pour, and M. Razeghi, "Demonstration of shortwavelength infrared photodiodes based on type-II InAs/GaSb/AlSb superlattices," *Appl. Phys. Lett.*, vol. 100, no. 21, p. 211101, 2012.

[7] Y. Wei *et al.*, "Uncooled operation of type-II InAs/GaSb superlattice photodiodes in the midwavelength," *Appl. Phys. Lett.*, vol. 86, no. 23, p. 233106, 2005.

[8] B. M. Nguyen, D. Hoffman, Y. Wei, P.-Y. Delaunay, A. Hood, and M. Razeghi, "Very high quantum efficiency in type-II InAs/GaSb superlattice photodiode with cutoff of 12 $\mu$m," *Appl. Phys. Lett.*, vol. 90, no. 23, p. 231108, 2007.

[9] Y. Wei, A. Gin, M. Razeghi, and G. J. Brown, "Advanced InAs/GaSb superlattice photovoltaic detectors for very long wavelength infrared applications," *Appl. Phys. Lett.*, vol. 80, no. 18, pp. 3262–3264, May 2002.

[10] Y. Wei, A. Gin, M. Razeghi, and G. J. Brown, "Type II InAs/GaSb superlattice photovoltaic detectors with cutoff wavelength approaching 32 $\mu$m," *Appl. Phys. Lett.*, vol. 81, no. 19, pp. 3675–3677, 2002.

[11] A. Haddadi, S. Ramezani-Darvish, G. Chen, A. M. Hoang, B.-M. Nguyen, and M. Razeghi, "High operability 1024×1024 long wavelength type-II superlattice focal plane array," *IEEE J. Quantum Electron.*, vol. 48, no. 2, pp. 221–228, Feb. 2012.

[12] R. Chevallier, A. Dehzangi, A. Haddadi, and M. Razeghi, "Type-II superlattice-based extended short-wavelength infrared focal plane array with an AlAsSb/GaSb superlattice etch-stop layer to allow near-visible light detection," *Opt. Lett.*, vol. 42, no. 21, pp. 4299–4302, 2017.

[13] A. Dehzangi, A. Haddadi, R. Chevallier, Y. Zhang, and M. Razeghi, "nBn extended short-wavelength infrared focal plane array," *Opt. Lett.*, vol. 43, no. 3, pp. 591–594, 2018.

[14] A. Haddadi, R. Chevallier, A. Dehzangi, and M. Razeghi, "Extended short-wavelength infrared nBn photodetectors based on type-II InAs/AlSb/GaSb superlattices with an AlAsSb/GaSb superlattice barrier," *Appl. Phys. Lett.*, vol. 110, no. 10, p. 101104, 2017.

[15] A. Haddadi, R. Chevallier, G. Chen, A. M. Hoang, and M. Razeghi, "Bias-selectable dual-band mid-/long-wavelength infrared photodetectors based on InAs/InAs$_{1-x}$Sb$_x$ type-II superlattices," *Appl. Phys. Lett.*, vol. 106, no. 1, p. 011104, 2015.

[16] L. Höglund *et al.*, "Influence of radiative and non-radiative recombination on the minority carrier lifetime in midwave infrared InAs/InAsSb superlattices," *Appl. Phys. Lett.*, vol. 103, no. 22, p. 221908, 2013.

[17] E. H. Steenbergen *et al.*, "Significantly improved minority carrier lifetime observed in a long-wavelength infrared III–V type-II superlattice comprised of InAs/InAsSb," *Appl. Phys. Lett.*, vol. 99, no. 25, p. 251110, 2011.

[18] B. V. Olson *et al.*, "Time-resolved optical measurements of minority carrier recombination in a mid-wave infrared InAsSb alloy and InAs/InAsSb superlattice," *Appl. Phys. Lett.*, vol. 101, no. 9, p. 092109, 2012.

[19] A. Haddadi, A. Dehzangi, S. Adhikary, R. Chevallier, and M. Razeghi, "Background–limited long wavelength infrared InAs/InAs$_{1-x}$Sb$_x$ type-II superlattice-based photodetectors operating at 110 K," *APL Mater.*, vol. 5, no. 3, p. 035502, 2017.

[20] A. Haddadi, A. Dehzangi, R. Chevallier, S. Adhikary, and M. Razeghi, "Bias–selectable nBn dual–band long–/very long–wavelength infrared photodetectors based on InAs/InAs$_{1-x}$Sb$_x$/AlAs$_{1-x}$Sb$_x$ type–II," *Sci. Rep.*, vol. 7, Jun. 2017, Art. no. 3379.

[21] A. Haddadi *et al.*, "High-performance short-wavelength infrared photodetectors based on type-II InAs/InAs$_{1-x}$Sb$_x$/AlAs$_{1-x}$Sb$_x$ superlattices," *Appl. Phys. Lett.*, vol. 107, no. 14, p. 141104, 2015.

[22] A. M. Hoang, G. Chen, R. Chevallier, A. Haddadi, and M. Razeghi, "High performance photodiodes based on InAs/InAsSb type-II superlattices for very long wavelength infrared detection," *Appl. Phys. Lett.*, vol. 104, no. 25, p. 251105, 2014.

[23] C. S. Kim *et al.*, "Molecular beam epitaxy growth of antimonide type-II 'W' high-power interband cascade lasers and long-wavelength infrared photodiodes," *J. Vac. Sci. Technol. B, Nanotechnol. Microelectron., Mater, Process,, Meas., Phenomena*, vol. 25, no. 3, pp. 991–994, 2007.

[24] B.-M. Nguyen, D. Hoffman, P.-Y. Delaunay, and M. Razeghi, "Dark current suppression in type II InAs/GaSb superlattice long wavelength infrared photodiodes with M-structure barrier," *Appl. Phys. Lett.*, vol. 91, no. 16, p. 163511, 2007.

[25] B.-M. Nguyen, S. Bogdanov, S. A. Pour, and M. Razeghi, "Minority electron unipolar photodetectors based on type II InAs/GaSb/AlSb superlattices for very long wavelength infrared detection," *Appl. Phys. Lett.*, vol. 95, no. 18, p. 183502, 2009.

[26] S. Maimon and G. W. Wicks, "*nBn* detector, an infrared detector with reduced dark current and higher operating temperature," *Appl. Phys. Lett.*, vol. 89, no. 15, p. 151109, 2006.

[27] A. Haddadi, G. Chen, R. Chevallier, A. M. Hoang, and M. Razeghi, "InAs/InAs$_{1-x}$Sb$_x$ type-II superlattices for high performance long wavelength infrared detection," *Appl. Phys. Lett.*, vol. 105, no. 12, p. 121104, 2014.

[28] H. Yang *et al.*, "Transfer-printed stacked nanomembrane lasers on silicon," *Nature Photon.*, vol. 6, pp. 615–620, Jul. 2012.

[29] Ka. Tanabe, K. Watanabe, and Y. Arakawa, "III–V/Si hybrid photonic devices by direct fusion bonding," *Sci. Rep.*, vol. 2, Apr. 2012, Art. no. 349.

[30] N. Li, K. Liu, V. J. Sorger, and D. K. Sadana, "Monolithic III–V on Silicon plasmonic nanolaser structure for optical interconnects," *Sci. Rep.*, vol. 5, Sep. 2015, Art. no. 14067.

[31] K. Takei *et al.*, "Nanoscale InGaSb heterostructure membranes on Si substrates for high hole mobility transistors," *Nano Lett.*, vol. 12, no. 4, pp. 2060–2066, 2012.

[32] H. Kim, A. C. Farrell, P. Senanayake, W.-J. Lee, and D. L. Huffaker, "Monolithically integrated InGaAs nanowires on 3D structured silicon-on-insulator as a new platform for full optical links," *Nano Lett.*, vol. 16, no. 3, pp. 1833–1839, 2016.

[33] D. Liang and J. E. Bowers, "Recent progress in lasers on silicon," *Nature Photon.*, vol. 4, pp. 511–517, Jul. 2010.

[34] J. A. Del Alamo, "Nanometre-scale electronics with III–V compound semiconductors," *Nature*, vol. 479, pp. 317–323, Nov. 2011.

[35] Y. H. Kim *et al.*, "Growth mode and structural characterization of GaSb on Si (001) substrate: A transmission electron microscopy study," *Appl. Phys. Lett.*, vol. 88, no. 24, p. 241907, 2006.

[36] S. H. Huang, G. Balakrishnan, A. Khoshakhlagh, L. R. Dawson, and D. L. Huffaker, "Simultaneous interfacial misfit array formation and antiphase domain suppression on miscut silicon substrate," *Appl. Phys. Lett.*, vol. 93, no. 7, p. 071102, 2008.

[37] R. Chevallier, A. Haddadi, and M. Razeghi, "Dark current reduction in microjunction-based double electron barrier type-II InAs/InAsSb superlattice long-wavelength infrared photodetectors," *Sci. Rep.*, vol. 7, Oct. 2017, Art. no. 12617.

[38] M. Zamiri *et al.*, "Indium-bump-free antimonide superlattice membrane detectors on silicon substrates," *Appl. Phys. Lett.*, vol. 108, no. 9, p. 091110, 2016.

[39] M. Zamiri *et al.*, "Antimonide-based membranes synthesis integration and strain engineering," *Proc. Nat. Acad. Sci. USA*, vol. 114, no. 1, pp. E1–E8, 2017.


**Yiyun Zhang** (M'17) received the M.S. degree from the Institute of Semiconductors, Chinese Academy of Sciences, in 2012, and the Ph.D. degree from the Department of Electrical and Electronic Engineering, The University of Hong Kong, in 2016. He is currently a Post-Doctoral Research Scientist with the Center for Quantum Devices, Northwestern University. His main research interests in Center for Quantum Devices include Sb-based type-II superlattice infrared photodetectors, focal plane arrays, epitaxial lift-off and large-area transfer of Sb-based thin-film devices onto Si for low-cost fabrication, and suppression of optical cross talk in dual-band type-II superlattice-based infrared photodetectors.

**Abbas Haddadi** received the Ph.D. degree in electrical engineering and computer science from Northwestern University, USA, in 2015. He is currently a Research Assistant Professor with Northwestern University. His current research interests include growth and characterization of III–V GaSb-based InAs/GaSb and InAs/InAsSb type-II superlattices photodetectors.

**Romain Chevallier** received the bachelor's degree from the Ecole Superieure de Physique et de Chimie Industrielles de la ville de Paris, France, and the master's degree in science and technology with a specialization in quantum devices and technology from University Paris Diderot. He is currently pursuing the Ph.D. degree in electrical engineering with Northwestern University. His Ph.D. research is with the Center for Quantum Devices, Northwestern University. His research focus is the processing of the infrared photodetectors based on InAs/GaSb and InAs/InAsSb type-II superlattices.

**Arash Dehzangi** (M'10) received the Ph.D. degree in nanoscience and nanoelectronics from University Putra Malaysia in 2012, specialization in scaling Si/III–V-based transistors and metal–oxide–semiconductor field-effect transistors (MOSFETs), focusing on junctionless Si nanowire transistors. He is currently a Research Scientist with the Center for Quantum Devices, Northwestern University, focusing on design and fabrication of III–V Sb-based optoelectronic devices and focal plan array camera systems. His main research interests include micro/nano fabrication, nanoelectronics, and design and processing of semiconductor electronic/optoelectronic devices, mostly Si and III–V-based MOSFETs, bipolar junction transistors, heterojunction phototransistors, and photodetectors. He is a member of the IEEE Society and the IEEE EDS.

**Manijeh Razeghi** (LF'17) received the Ph.D. degree in physics from the University of Paris, Paris, France, in 1980. From 1980 to 1991, she was with Thomson-CSF, Orsay, France, first as a Senior Research Scientist and then as the Head of the Exploratory Materials Laboratory. Since 1991, she has been a Walter P. Murphy Professor and the Director of the Center for Quantum Devices, Northwestern University, Evanston, IL, USA, where she started the undergraduate and graduate program in solid-state engineering. She developed and implemented modern metal-organic chemical vapor deposition (MOCVD) epitaxial growth for the entire compositional ranges of III–V semiconductors and heterostructures. She realized the first InP quantum wells and superlattices and demonstrated the marvels of quantum mechanics in the low-dimensional world. Her pioneering work on InP-based compound semiconductors culminated in the 1989 publication, *The MOCVD Challenge Volume 1: A Survey of GaInAsP-InP for Photonic and Electronic Applications*. She is one of the leading scientists in the field of semiconductor science and technology, pioneering in the development and implementation of major modern epitaxial techniques. She has authored or co-authored over 1000 research papers, 12 books, and over 30 book chapters. She holds 30 U.S. patents and has given more than 1000 invited and plenary talks. Her current research interests include nanoscale optoelectronic quantum devices. She received the International Business Machines Corporation Europe Science and Technology Prize in 1987, the Achievement Award from Society of Women Engineers (SWE) in 1995, the R.F. Bunshah Award in 2004, the Jan Czochralski Gold Medal in 2016, the Benjamin Franklin Medal in Electrical Engineering in 2018, and many best paper awards. She has been an Elected Fellow of SWE since 1995, the Society of Photo-Optical Instrumentation Engineers since 2000, the International Engineering Consortium since 2003, the Optical Society of America since 2004, the American Physical Society since 2004, and the Institute of Physics since 2005. She also has been an Elected Lifetime Fellow of the Materials Research Society since 2008.